Fabrication of Photo-carrier Transfer Channel for Near Infrared Up-conversion Coupled Photocathode Via Sandwiched-like Nanostructure

XiChen, Yuyu Bu*, HuanLi, XiaoWang, Jin-Ping Ao

Key Laboratory of Wide Band-Gap Semiconductor Materials and Devices, School of Microelectronics, Xidian University, Xi'an, 710071, China. mail: yybu@xidian.edu.cn

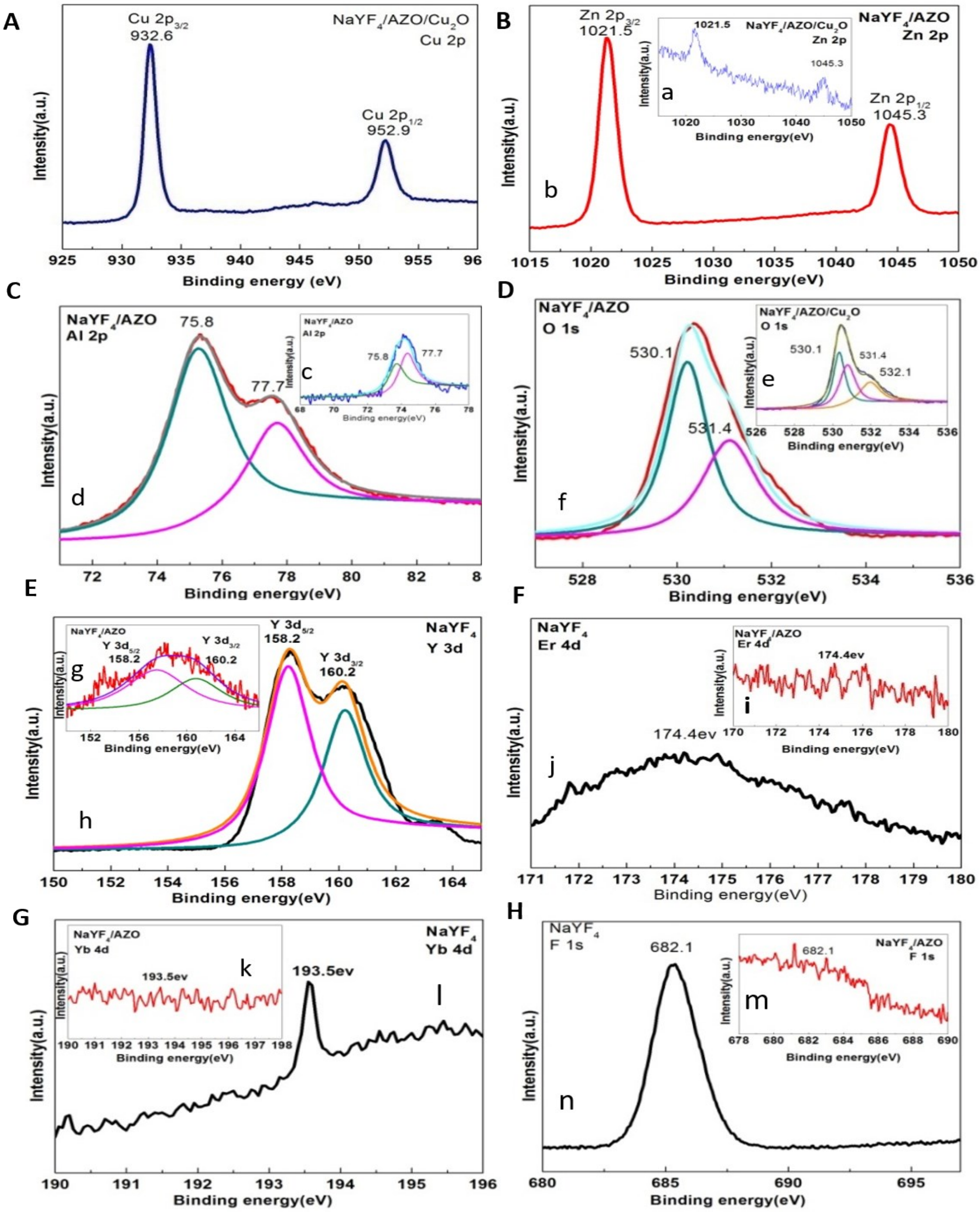

Figure S1. XPS spectra depicting peaks due to A) Cu 2*p*, B) Zn 2*p*, C) Al *2p*, D) O 1*s*, E) Y 3*d,* F) Er 4*d*, G) Yb 4*d*, H) F 1*s* in $NaYF_4:Er^{3+}-Yb^{3+}/AZO/Cu_2O$ sandwiched-like composite thin film.

Fig.S1 shows the X-ray photoelectron spectroscopy (XPS) survey spectra of Cu, Zn, Al, O elements in $NaYF_4$:Er^{3+}-Yb^{3+}, $NaYF_4$:Er^{3+}-Yb^{3+}/AZO, and $NaYF_4$:Er^{3+}-Yb^{3+}/AZO/Cu_2O composite films. **Fig. S1A** is the XPS spectra of Cu 2*p* in $NaYF_4$:Er^{3+}-Yb^{3+}/AZO/Cu_2O sandwiched-like composite thin film, the Cu $2p_{3/2}$ and Cu $2p_{1/2}$ can be observed at 932.6 eV and 952.9 eV, respectively. In **Curve S1a**, the $NaYF_4$:Er^{3+}-Yb^{3+}/AZO/Cu_2O sandwiched-like composite thin film shows the presence of Zn *2p* at 1021.5 eV and 1045.3 eV, and the peaks of Zn *2p* in $NaYF_4$:Er^{3+}-Yb^{3+}/AZO composite thin film are shown in **Curve S1b**, the **Fig.S1B** indicates the Zn *2p* comes from AZO only. As shown in **Curve S1c** and **Curve S1d**, Al *2p* can be observed at 75.8 eV and 77.7 eV, **Fig. S1C** indicates that Al *2p* comes from AZO only. Due to Cu-O bonds, Zn-O bonds and Al-O bonds, in **CurveS1e** the presence of O *1s* is observed on $NaYF_4$:Er^{3+}-Yb^{3+}/AZO/Cu_2O at 530.1 eV, 531.4 eV and 532.1 eV, respectively, and in **CurveS1f**, O*1s* peaks can be observed on $NaYF_4$:Er^{3+}-Yb^{3+}/AZO at 530.1 eV, 531.4 eV, attribute to Zn-O bonds and Al-O bonds. The **Fig. S1D** indicates that there are only ZnO, Cu_2O and Al_2O_3 exist in $NaYF_4$:Er^{3+}-Yb^{3+}/AZO, and $NaYF_4$:Er^{3+}-Yb^{3+}/AZO/Cu_2O composite films. In $NaYF_4$:Er^{3+}-Yb^{3+} thin film, the peaks at 158.2 eV and 160.2 eV contributed by Y$3d_{5/2}$and Y$3d_{3/2}$ can be seen in **Curve S1g**, in$NaYF_4$:Er^{3+}-Yb^{3+}/AZO composite film, the peaks are in same location shown by **Curve S1h**, the **Fig. S1E** certify the existence of $NaYF_4$. As shown in **Curve S1i**, the peak of Er*4d* in $NaYF_4$:Er^{3+}-Yb^{3+}/AZO composite film is obscured, in $NaYF_4$:Er^{3+}-Yb^{3+} thin film, the peaks at 174.4 eV contributed by Er*4d* can be seen in **Curve S1j**, the **Fig.S1F** certify that the Er element has been doped in $NaYF_4$ successfully. In **Curve S1k** the peak of Yb*4d* in $NaYF_4$:Er^{3+}-Yb^{3+}/AZO composite film is obscured, in $NaYF_4$:Er^{3+}-Yb^{3+} thin film, the peaks at 174.4 eV contributed by Er*4d* can be seen in **Curve S1j**, the **Fig S1G** certify that the Yb element has been doped in $NaYF_4$ successfully. The **Fig. S1H** indicates the existence of F.

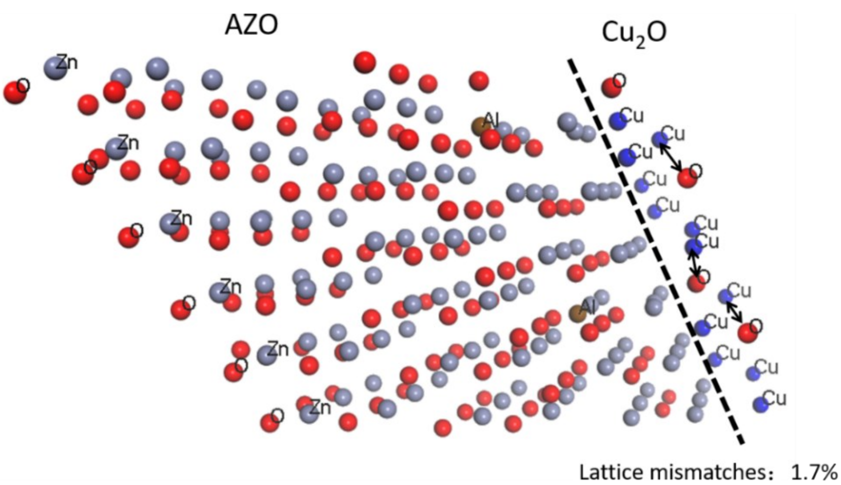

Figure S2. The lattice mismatch between AZO and Cu_2O.

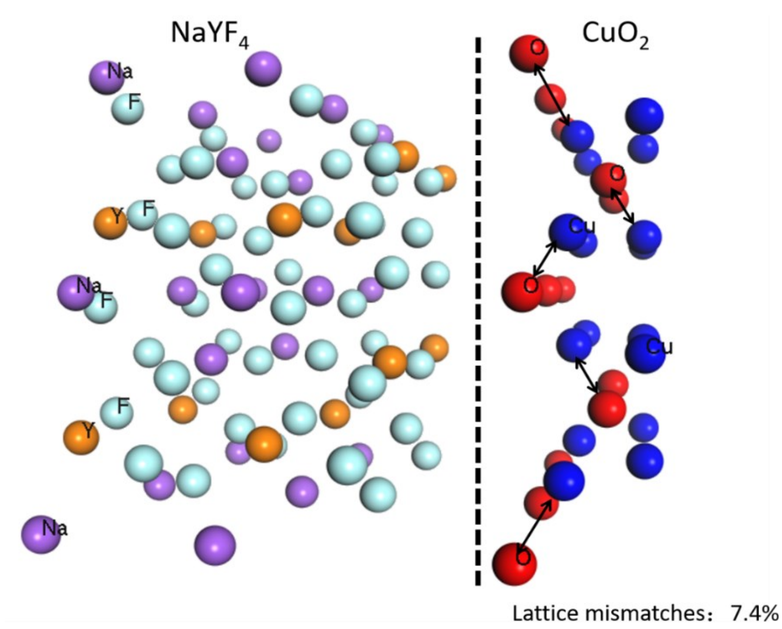

Figure S3. The lattice mismatch between $NaYF_4$ and Cu_2O.

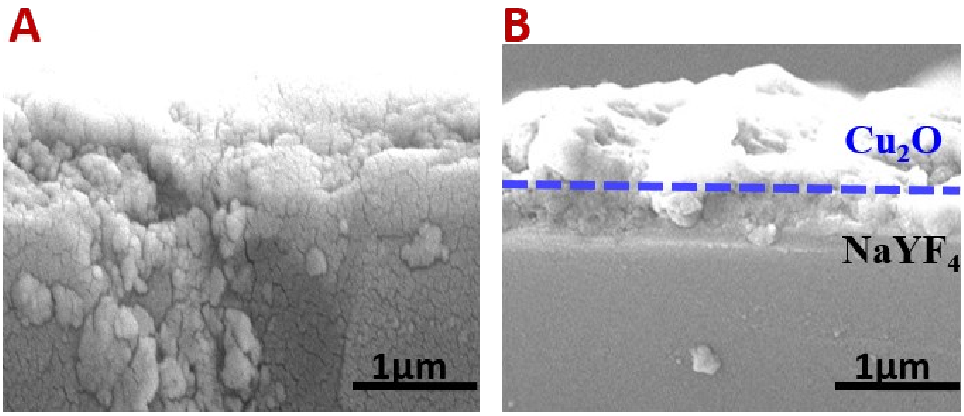

Fig. S4. A) Cross-section SEM image of $NaYF_4$:Er^{3+}-Yb^{3+}thin film. B) Cross-section SEM mapping of $NaYF_4$:Er^{3+}-Yb^{3+}/Cu_2O composite thin film.

Fig.S4 shows the cross-section SEM image of $NaYF_4$:Er^{3+}-Yb^{3+} film and $NaYF_4$:Er^{3+}-Yb^{3+}/Cu_2O composite thin film, respectively. The Cu_2O above the $NaYF_4$:Er^{3+}-Yb^{3+} has been deformation.

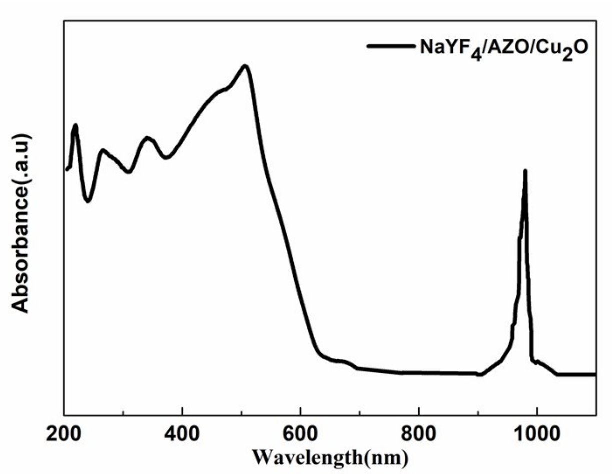

Figure S5. The UV-Vis of the $NaYF_4$/AZO/Cu_2O composite film.

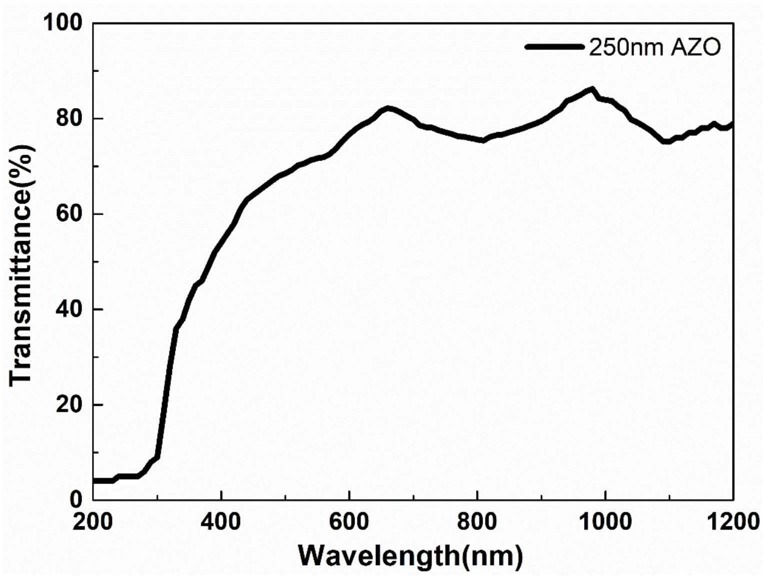

Figure S6. Transmission spectra of the 250 nm AZO film.

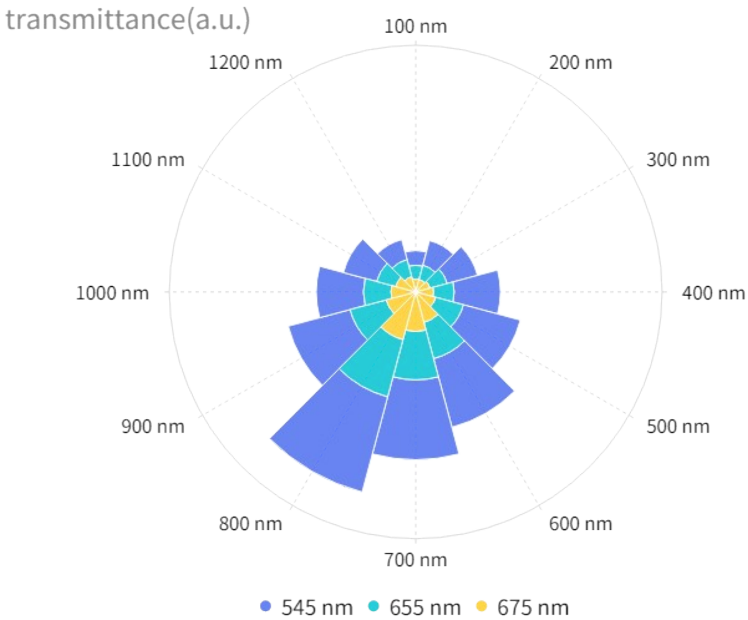

on float glass.

Figure S7. The UC fluorescence intensity of $NaYF_4$:Er^{3+}-Yb^{3+} thin films with different thickness.

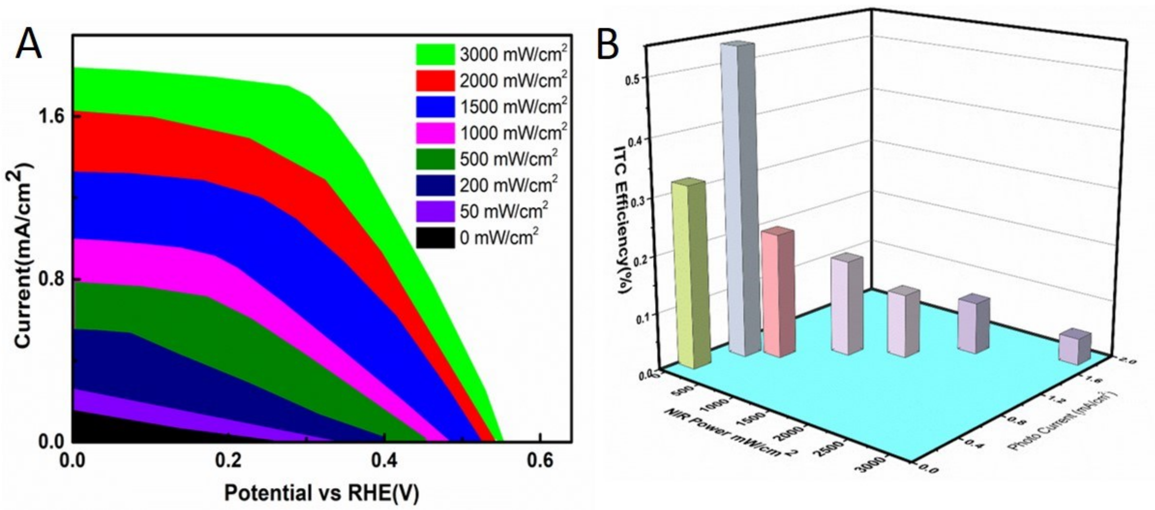

Fig. S8. A) I-V curves of $NaYF_4$:Er^{3+}-Yb^{3+}/AZO/Cu_2O composite film were measured in 0.1M Na_2SO_4 (pH=6.1). B) ITC of $NaYF_4:Er^{3+}$-Yb^{3+}/AZO/Cu_2O composite film.

Fig.S8A is the photo-induced I-V curve of $NaYF_4:Er^{3+}$-Yb^{3+}/AZO/Cu_2O photocathode by continuous 980 nm NIR excitation with different power density (0W excitation power means light off). **Fig.S8B** is the ITC efficiency of the $NaYF_4:Er^{3+}$-Yb^{3+}/AZO/Cu_2O photocathode with different NIR power density. The ITC depend on photoelectric conversion efficiency, the maximum ITC efficiency of the $NaYF_4:Er^{3+}$-Yb^{3+}/AZO/Cu_2O photocathode is 0.56% with 200 mW/cm^2 NIR excitation power. The Nernst **equation (1)** can convert potential vs. Ag/AgCl into the RHE potential. The ITC was calculated from the I-V curve with **equation (2)** in **Fig.S8B**, the I means the photocurrent, V is the bias voltage, and P_{light} means the NIR excitation power.

$$E_{RHE} = E_{Ag/AgCl} + 0.059\,pH \qquad (1)$$

$$ITC(\%) = \frac{\int_{V_{RHE}} I\,dV - \int_{V_{RHE}} I_{dark}\,dV}{P_{light}} \qquad (2)$$

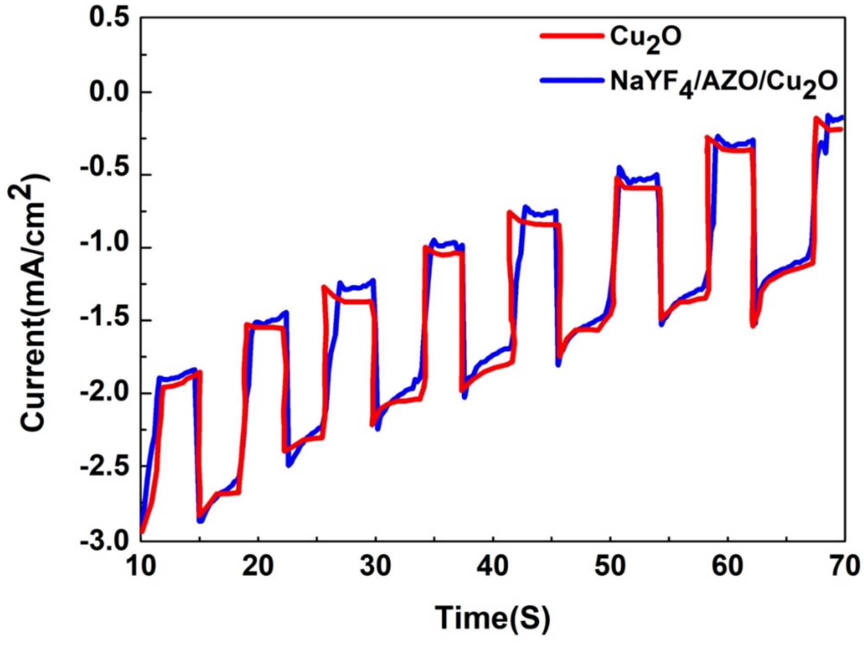

FigureS9. I-T curves of $NaYF_4:Er^{3+}$-Yb^{3+}/AZO/Cu_2O photocathode and Cu_2O photocathode by sunlight from a Xe lamp.

Fig. S9 is the photo-induced I-T curves of $NaYF_4:Er^{3+}$-Yb^{3+}/AZO/Cu_2O and Cu_2O photocathodes at bias potential 0.5 V by sunlight on/off. The Cu_2O is not stable in sunlight, it caused the dark photocurrent has been increased. The percentage of 980 nm photon is very low in solar spectrum, so the PEC performance only can be limitedly improved.

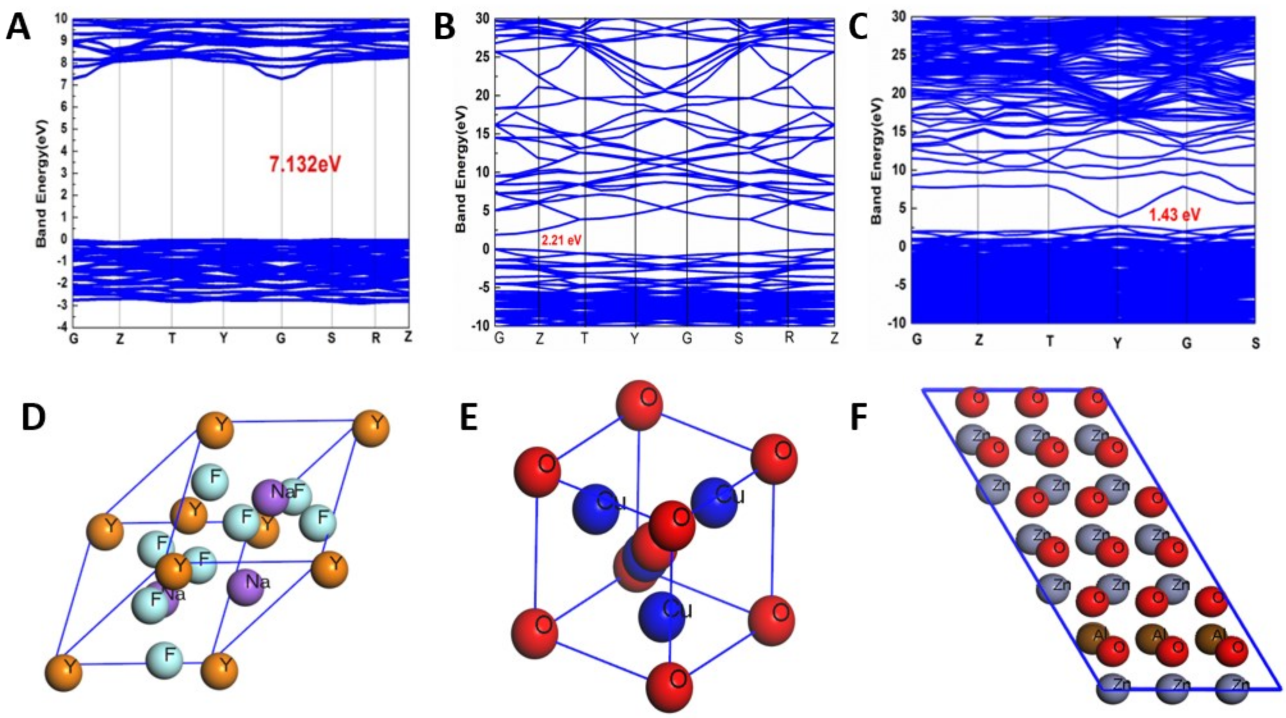

Fig. S10. A-C) The DOS of $NaYF_4$, Cu_2O and AZO. D-F) The crystal structure of$NaYF_4$and Cu_2O, AZO.

The Density of State (DOS) of $NaYF_4$:Er^{3+}-Yb^{3+}, AZO and Cu_2O and corresponding crystal structure has been showed in **Fig S10.** According to **equation (3)**, the electron effective mass has been calculated, the E is the bottom of conduct band.

$$m_{e*} = h^2 \left(\frac{d^2 E}{d^2 \kappa} \right)^{-1} \tag{3}$$